All-polymer nanocomposites having superior strength, toughness and ultralow energy dissipation

Haixiao Wan [a,1], Sai Li [a,1], Yachen Wang [a], Zhudan Chen [b], Junwei He [a], Chunhua Li [c], Gengxin Liu [c], Jun Liu [a,*], Xiaodong Wang [a,*], Thomas P. Russell [e,f,**], Liqun Zhang [a,d,***]

[a] State Key Laboratory of Organic-Inorganic Composites, Beijing University of Chemical Technology, Beijing 100029, China
[b] Institute of Automation, Beijing University of Chemical Technology, Beijing 100029, China
[c] State Key Laboratory for Modification of Chemical Fibers and Polymer Materials, Center for Advanced Low-dimension Materials, Donghua University, Shanghai 201620, China
[d] Institute of Emergent Elastomers, School of Materials Science and Engineering, South China University of Technology, Guangzhou 510641, China
[e] Polymer Science and Engineering Department, University of Massachusetts Amherst, 120 Governors Drive, Amherst, MA 01003, USA
[f] Materials Sciences Division, La wrence Berkeley, National Laboratory, Berkeley, CA 94720, USA

A B S T R A C T

Toughening polymers has attracted significant interest. Traditionally, polymer toughness is enhanced by constructing polymer networks or introducing sacrificial bonds into the chains between crosslink points. These strategies, though, introduce pronounced energy dissipation and associated heat, both of which are undesirable under long-term cyclic loading, for example at the interface of implants in the human body. By incorporating single-chain nanoparticles (SCNPs) into linear polymer chains to generate all-polymer nanocomposites (APNCs), we have been able to achieve high strength, high toughness with low energy dissipation. Using a combination of simulation and experimental results, we are advancing a "SCNPs effect" where tightly cross-linked SCNPs produce a modulus contrast to achieve strengthening and toughening. Benefitting from the soft interface, the penetrable and deformable SCNPs cause the surrounding polymer chains to move in concert, significantly reducing the interfacial friction to achieve low energy dissipation. The intramolecular cross-linking of the SCNPs and adhesion between the SCNPs and polymer matrix are critical for realizing such high-performance systems. Based on a Gaussian regression model and back propagation (BP) neural network, the mechanical strength can be predicted and is supported by simulations. The APNC concept described can be applied to elastomers and gels, broadening its utilization in high-cycle and low-dissipation applications, like soft robots, flexible sensors and cartilage replacements, and artificial heart valves.

1. Introduction

Polymer nanocomposites (PNCs) are a class of materials that pose interesting fundamental scientific challenges and potential engineering applications in materials science [1–5], biophysics and medicine [6–9]. Manipulating their mechanical and viscoelastic properties has attracted significant interest, since their poor mechanical properties, brittleness and high energy-dissipation seriously limit the scope for their applications. Traditional PNCs are obtained by embedding rigid inorganic nanoparticles (NPs) such as carbon black, graphene and carbon nanotubes, to improve the mechanical strength [10,11]. However, the enhanced mechanical strength is often accompanied by inferior toughness, resulting in a trade-off between strength and toughness [12,13]. Significant efforts have been made to simultaneously improve both by incorporating effective energy dissipation mechanisms [14–20], including sacrificial and dynamic covalent bonds. Nevertheless, they inevitably exhibit more pronounced hysteresis loss under the cyclic tension and recovery, since high toughness often means that much

* Corresponding authors.
** Corresponding author at: Polymer Science and Engineering Department, University of Massachusetts Amherst, 120 Governors Drive, Amherst, MA 01003, USA.
*** Corresponding author at: State Key Laboratory of Organic-Inorganic Composites, Beijing University of Chemical Technology, Beijing 100029, China.
E-mail addresses: liujun@mail.buct.edu.cn (J. Liu), wangxdfox@aliyun.com (X. Wang), russell@mail.pse.umass.edu (T.P. Russell), zhanglq@mail.buct.edu.cn (L. Zhang).
[1] The authors contribute equally to this paper.

energy need to be dissipated to resist the crack propagation (Scheme 1). This poses major obstacles for their use in applications involving cyclic loading conditions, as for example with soft robots, actuators, cartilage replacements and artificial heart valves. Consequently, the pursuit of high-performance PNCs that combine high strength, high toughness, and low energy dissipation has been crucial.

Advances in the single-chain technology have made it possible to produce macromolecular architectures by the manipulation of single polymer chains [21]. Single-chain nanoparticles (SCNPs) has become a rapidly growing research topic due to their unique advantages, such as design flexibility, excellent biocompatibility, and potential applications in catalysis [22–25], sensors [26–29], and nanomedicines [29–33]. These NPs are produced by intramolecular cross-linking using reactive functional sites along the individual polymer chains, mimicking, to a first approximation the self-folding behavior of biomacromolecules [29, 34–37]. The feasibility of preparing SCNPs and the characterization of the SCNPs has been demonstrated in many recent works [38], providing a platform for designing and fabricating novel SCNPs [39–41]. The na- ture of the individual polymer chain precursors varies from soft to hard by adjusting the degree of intramolecular cross-linking of the SCNPs, resulting in a transformation of the PNCs from an unfilled purely linear polymer chains blend to a conventional PNCs with rigid NPs. Further- more, the SCNPs can endow a unique structure and performance to the PNCs, different from conventional PNCs filled with rigid NPs. Mackay et al. [42–45] found that there was a remarkable non-Einstein-like decrease in the viscosity by introducing organic polystyrene (PS) NPs into the linear PS chains [42,44]. This phenomenon is completely different from conventional PNCs, where the viscosity increases with increasing rigid NPs contents. The reduction in the viscosity increases with increasing chain length of polymer matrix. This can be explained by the reduced friction of polymer segment blobs having the comparable size and interacting directly with the SCNPs [46]. The structure and dynamics of the all-polymer nanocomposites were systematically studied by Qian and co-workers [47–50]. The smooth density distribution of polymer chains along the radial direction of the NP implies a liquid-liquid like interfacial contact, and an acceleration of segmental relaxation in the vicinity of the NP surface were observed, primarily due to the soft nature and the deformability in the shape of the SCNPs. Moreno et al. [51] argued that the soft SCNPs were fully penetrated by the polymer chains leading to only topological constraints without the geometrical confinement caused by rigid NPs. A theoretical model was proposed to understand how the soft permeable NPs diffuse in the unentangled and entangled polymer liquids [52]. The effects of NPs softness, molecular weight of linear matrix chain, and temperature on the diffusion of soft NPs were precisely examined. Briefly, the incorpo- ration of soft, penetrable and deformable SCNPs enables the all-polymer nanocomposites to possess unique properties. However, up to now, no effort has been made to explore the mechanical and viscoelastic prop- erties of the all-polymer nanocomposites.

With these in mind, we are advancing a new strategy to tailor the mechanical and viscoelastic properties of the all-polymer nanocomposites by employing SCNPs to produce high-performance PNCs with high strength, high toughness and low energy dissipation. The size of the SCNPs is nanoscale, that will enhance the nano-reinforcing effect, and SCNPs are soft and deformable, that will enhance toughening. Moreover, the internal structure of the SCNPs can be varied from loose to tight by tailoring the degree of intramolecular cross-linking, leading to SCNPs with a mechanical strength that will exceed that of the polymer matrix and, therefore, a modulus contrast expected to produce high strength and toughness [52], since the bond rupture within SCNPs can prevent the catastrophic crack propagation under loading. The proper- ties of the traditional PNCs are often determined by a combination of enthalpic and entropic contributions, which makes it extremely difficult to control the dispersion of the NPs in the matrix and interfacial inter- action. However, there are favorable enthalpic interactions between the NPs in the all-polymer nanocomposites, in which the NPs have no “hard” components but are fully polymer-based components. A good dispersion of the NPs is achieved, since the matrix chains can penetrate the NPs [42, 51]. Generally, SCNPs show excellent dispersion in the matrix, and, depending on the degree of cross-linking, can be penetrated by the surrounding polymer matrix chains to produce a soft interface. The reversible deformation of SCNPs can store and release energy so that the surrounding polymer chains move together with the SCNP during the loading and unloading process, suppressing interfacial slippage and reducing the interfacial friction, so as to decrease hysteresis.

Here, we present a systematic experimental and coarse-grained molecular dynamics (MD) simulation study to investigate all-polymer nanocomposites using SCNPs. The energy dissipation of the all-polymer nanocomposites is simulated by tension-recovery deformation, as described in our previous work [53,54]. We find that SCNPs serve as a good candidate for balancing the mechanical and viscoelastic performance of PNCs to improve strength, toughness and suppress hysteresis simultaneously (Scheme 1). This can be realized by manipu- lating the intramolecular cross-linking of the SCNPs and the interfacial adhesion between the SCNPs and polymer matrix, which is impossible to be realized with conventional PNCs filled with rigid NPs. Based on a

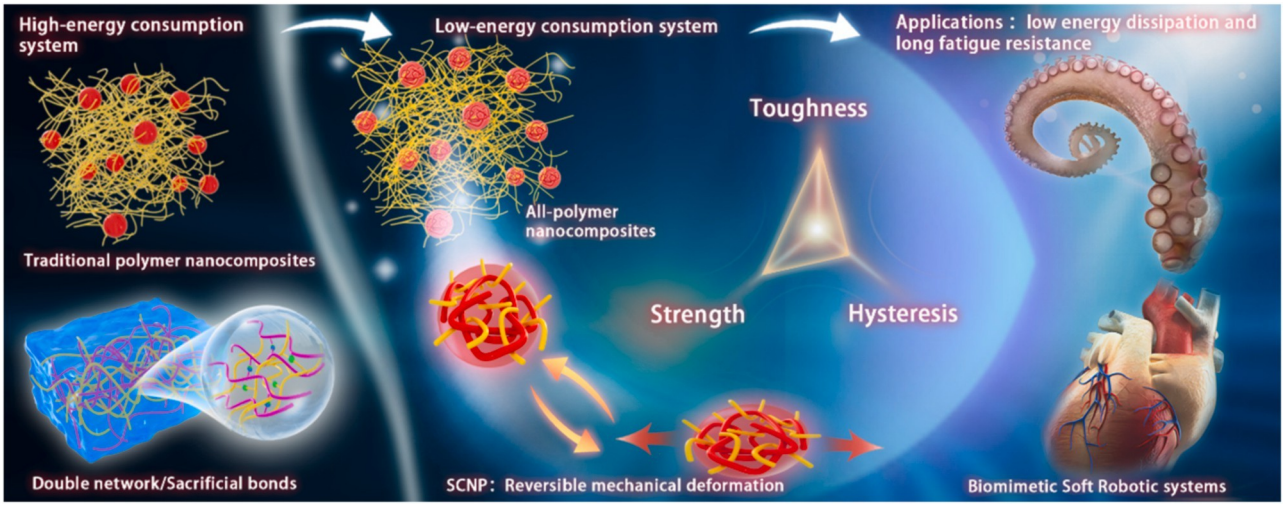

Scheme 1. The schematic diagram for exploiting high-strength, high-toughness and low-hysteresis materials based on the all-polymer nanocomposites. This novel PNCs is suitable for materials with low energy dissipation and long fatigue resistance, such as soft robots, flexible sensors, cartilage replacements, and artificial heart valves.

Gaussian regression model and a back propagation (BP) neural network, along with simulations, we predict the mechanical strength as a function of the degree of intramolecular cross-linking of the SCNPs. The findings in this work provide a new methodology for the design and fabrication
of high-cycle, low-dissipation PNCs, applicable to soft robots, flexible sensors, cartilage replacements, and artificial heart valves (Scheme 1).

2. Materials and methods

2.1. Simulation model and methods

In our all-polymer nanocomposites, SCNPs and matrix chains were modeled via coarse-grained molecular dynamics (CGMD) simulation using Kremer-Grest bead-spring model [55], where the monomeric units of SCNPs and matrix chains were represented by beads of mass m and diameter σ. The coarse-grained (CG) process maps the atomistic system of reference into a coarser mesoscopic model, neglecting the chemical characteristics of the chains, where several atoms are combined together in a simplified way to reduce the interaction sites thus speeding up the calculations. The CG models maintain the main physics underpinning of their structural, dynamical, and mechanical properties. In the past de- cades, several CG models had successfully reproduced the properties of specific polymer systems, including poly (vinyl alcohol) [56], poly- ethylene [57–60], polypropylene [60], and polystyrene [61,62].

The matrix chain length was 200 in our simulations, which was longer than the entanglement length ($N_e \approx 65 \pm 7$) for this model [63]. The precursor of each SCNP was a linear polymer chain with the degree of polymerization equal to 500. The potential cross-linking sites were evenly distributed on the backbone of the linear polymer chains ac- cording to the target degree of cross-linking (10%, 20%, 30% and 50%), and they were randomly combined in pairs to realize the intramolecular cross-linking of each SCNP (Fig. 1a). The intramolecular cross-linking degree for each SCNP was calculated by the fraction of cross-linking sites contained in each precursory linear chain. The PNCs with the de- grees of intramolecular cross-linking of SCNPs equal to 10%, 20%, 30% and 50% denote as 10%-SCNP, 20%-SCNP, 30%-SCNP and 50%-SCNP,
respectively. The total number of polymer beads for each simulation system was 20000. Eight SCNPs were introduced into each simulation system, corresponding to the weight fraction of NPs of 20%. Since all beads in the system have the same size and mass, the volume fraction is identical to the weight fraction. For comparative analysis, the conven- tional PNCs system filled with completely rigid NPs was also con- structed, in which the NPs were modeled as rigid bodies and the bonded energy (in Eq. (2)) of intra-NP was not considered here in order to achieve NP conformations as compact as possible. The characteristic of rigid NPs is not deformable, like hard NPs. The non-bonded interaction between any two beads was modeled by the shifted Lennard-Jones (LJ) potential:

$$U(r) = \begin{cases} 4\varepsilon\left[\left(\frac{\sigma}{r}\right)^{12} - \left(\frac{\sigma}{r}\right)^{6}\right] + U_{shift} & r \le r_{cutoff} \\ 0 & r > r_{cutoff} \end{cases} \quad (1)$$

where ε is the pair interaction energy scale and r is the distance between the two interaction sites of the center of mass. U_{shift} is a constant to guarantees the continuity of the interaction at the cutoff distance. To ensure the formation of the globular SCNPs and realize the intra- molecular cross-linking process, the interaction strength of the cross- linking sites on the linear precursor was set to be strong attractive, $\varepsilon_{cross} = 5.0$ and $r_{cutoff} = 2.5\sigma$ before the cross-linking process finished. After the intramolecular cross-linking was completed, the interaction strength between the cross-linking sites was changed to be $\varepsilon_{cross} = 1.0$. Except for this case, the interactions between the other polymer beads were always set to be attractive with $\varepsilon = 1.0$ and $r_{cutoff} = 2.5\sigma$. More- over, two types of bonded interaction between two consecutive beads were adopted to characterize different mechanical properties, depending on the tensile condition. The harmonic bond potential was used for obtaining mechanical strength and hysteresis under uniaxial loading, cyclic loading-unloading as well as dynamic shear tests:

$$U_{bond} = \frac{1}{2}K(r - r_0)^2 \quad (2)$$

where $K = 200.0\varepsilon/\sigma^2$ is the spring constant. The equilibrium bond dis- tance r_0 was set as 1.0σ. In addition, the quartic bond potential was used to achieve mechanical toughness to allow covalent bonds to break under the triaxial tensile tests:

$$U(r) = \begin{cases} k(y - b_1)(y - b_2)y^2 + U_0 & r < r_c \\ U & r > r_c \end{cases} \quad (3)$$

where $y = r - \Delta r$ is the shift of the quartic center compared to its initial position and $\Delta r = r_c = 1.5\sigma$ is the broken distance beyond which bonds are broken permanently. The other parameters were $k = 1434.3\varepsilon/\sigma^4$, $b_1 = -0.759\sigma$, $b_2 = 0.0$, and $U_0 = 67.223\varepsilon$. The quartic bond potential has been widely employed to investigate the fracture toughness of polymer materials [64,65].

Three-dimensional periodic boundary conditions were adopted to eliminate edge effects in the simulation. The NVT and NPT ensemble were applied to equilibrate the simulated systems by using the Nos´e - Hoover thermostat and barostat with normal temperature $T^* = 1.0$ and pressure $P^* = 1.0$. The simulated temperature $T^* = 1.0$ is far from above the glass transition temperatures (T_g) of our simulated systems (Fig. S2),
indicating that all systems are at a rubbery state. The velocities and positions of the beads were updated each $\Delta t = 0.001\tau$ by time integration utilizing the velocity-Verlet algorithm, where τ represents the LJ time unit $\tau = (m\sigma^2/\varepsilon)^{1/2}$.

Our simulation protocol is to introduce high-T_g SCNPs as nano-fillers into low-T_g the polymer matrix chains (Fig. S3) to construct the all-polymer nanocomposites, consisting of four steps: equilibrium, intra-molecular cross-linking of SCNPs, replication and re-equilibrium. The detailed steps were described as follows: (i) the simulations were started from a non-overlapped configuration of a linear precursor of SCNP and 10 polymer matrix chains in a large simulation box. They were equilibrated over 4×10^6 time steps under NVT ensemble without allowing the intramolecular cross-linking of SCNPs. Correspondingly, the linear precursor generated the collapsed structure due to the strong attractive interaction of the cross-linking sites. (ii) In the next step, the intra-molecular cross-linking process of the SCNPs was implemented under the same NVT conditions by randomly selecting pairs of the cross-linking sites within a distance of 2.0σ. It is noteworthy that the cross-linking process was monofunctional and irreversible. A cross-linking site was only allowed to bond to another cross-linking site. If there was more than one candidate of cross-linking site for any given cross-linking site, one of the candidate sites was chosen at random to form a bond. Once a bond was created, a harmonic potential (in Eq. (2)) was introduced between the two cross-linking sites. The cross-linking process was repeated until the degree of cross-linking was within 0.5% of target degree of cross-linking. Similar algorithms for generating SCNP by the intramolecular cross-linking have been adopted extensively by other MD

simulations [39,51,66]. For each degree of cross-linking, we changed the random seeds for initial velocities of the cross-linking process to get different initial configurations. Unless otherwise stated, the simulated results were averaged more than three independent initial configura- tions. (iii) After the cross-linking process was completed, the replicate command was used to enlarge the system, which was eight times larger than the above system. This means that there were eight SCNPs and 80 matrix polymer chains in the final simulation box. (iv) The obtained all-polymer nanocomposites were equilibrated under the NVT ensemble (5×10^6 time steps) to release the local stress and expand morphologies for all systems. Then, the NPT ensemble was applied to further equili- brate all systems so as to increase the number density of polymer beads,

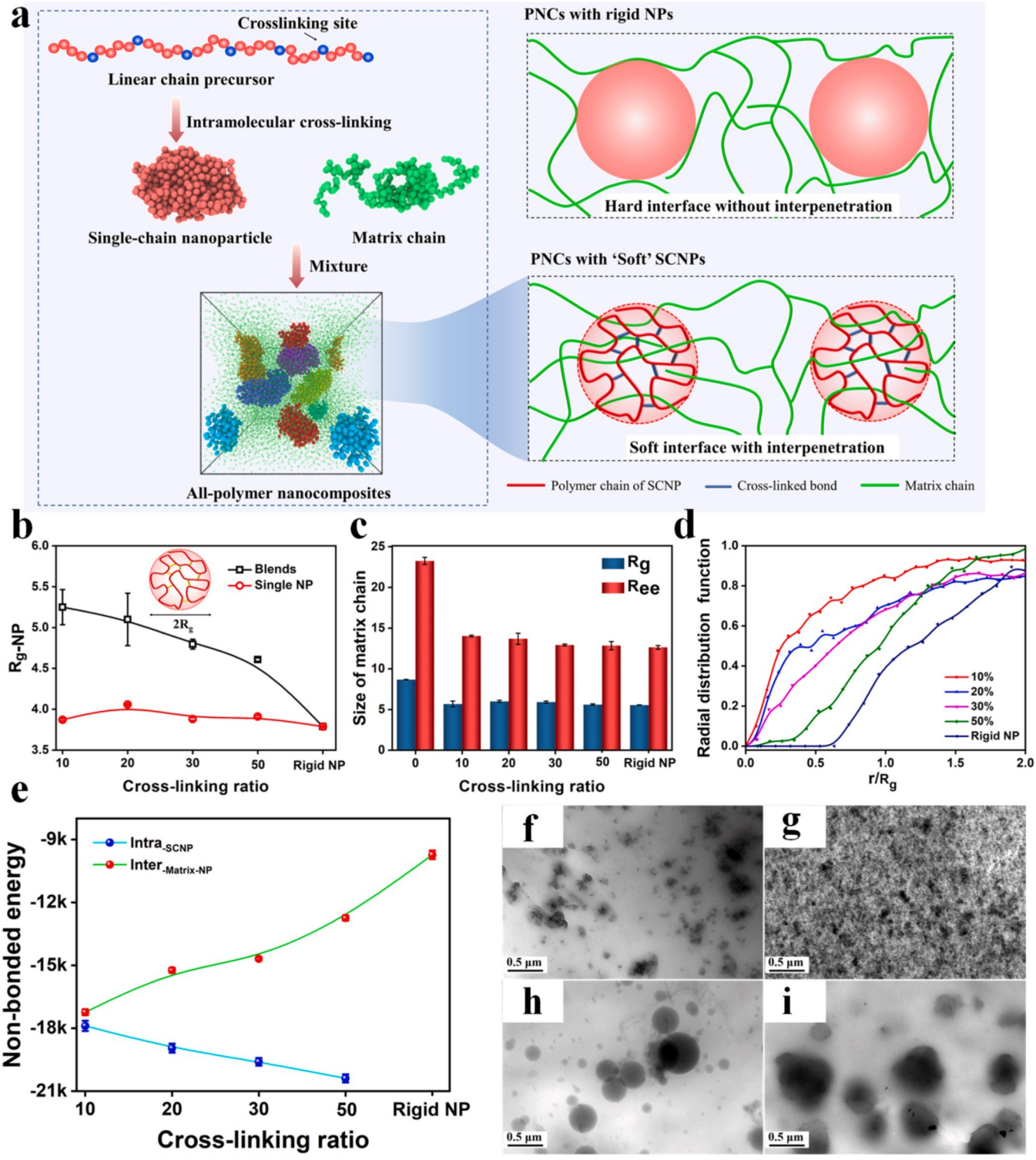

Fig. 1. (a) Schematic representation of the all-polymer nanocomposites consisting of the intramolecular cross-linked SCNPs and linear matrix chains. The SCNPs are produced from the precursors of linear chain with the cross-linking sites on the backbone. Green dots represent matrix chains and among other different colors, each color represents a SCNP in the left snapshot. The SCNPs can be penetrated by the surrounding polymer matrix chains to produce a soft interface whereas the rigid NPs can not be interpenetrated and only contact with the matrix chains on their surface (right). (b) Radius of gyration for SCNPs in blends and single SCNP as a function of the degree of intra-chain cross-linking. Error bars for the single SCNPs are smaller than the symbol size. (c) Radius of gyration and end-to-end distance for matrix chains vs the degree of intra-chain cross-linking. (d) Radial distribution function (RDF) between the center-of-mass of SCNPs and the monomers of matrix chains. (e) Intramolecular non-bonded interaction energy of SCNPs and intermolecular non-bonded interaction energy between matrix chains and SCNPs under different degrees of cross-linking in the equilibrium state. TEM images of (f) SiO_2-50/SBR (10% wt), (g) PS NP/SBR (10% wt), (h) SiO_2-300/SBR (20% wt), (i) SBR NP/SBR (20% wt).

keeping it around a reasonable value $\rho^* = 0.92$, which was in good agreement with either atomistic [67] or other CG simulations [61,62]. Each simulation system was equilibrated over a long time (12×10^6 time steps) to ensure that each polymer chain had moved at least $2R_g$ (R_g was the root-mean-square radius of gyration of polymer chains). After sufficient equilibrium, a simulation running of 6×10^6 time steps were implemented for data collection. The pressure and the volume versus the simulation time with various degrees of intramolecular cross-linking imply that the well-equilibration systems have been achieved (Fig. S4). We collected the structure and dynamics data for ensemble average, and the statistical error bars were included to indicate the standard deviation of data.

Mechanical strength was computed by employing a uniaxial deformation for all simulated systems. The uniaxial tension was implemented via deforming the periodic box along the X axis at a constant displace- ment rate accompanied by the Y and Z directions simultaneously adjusted to maintain the simulation box constant, which corresponds to the fact that the elastomers are often incompressible with its Poisson's ratio $\mu \approx 0.5$. The average tensile stress was described from the devia- toric part of the stress tensor:

$$\sigma = (1 + \mu)(-P_{XX} + \frac{P}{2}) \cong \frac{3}{2}(-P_{XX} + P) \quad (4)$$

where $P = \Sigma_i P_{ii}/3$ is the hydrostatic pressure and P_{XX} is the normal pressure component in the strain direction. The tensile strain was calculated from the ratio of instantaneous length $L_x(t)$ -L_x to the initial length of periodic box L_X along the applied displacement axis. The engineering strain rate was set to be $\dot{\varepsilon} = (L_x(t) - L_x)/L_x/\tau = 0.0327/\tau$, which was one of the strain rates widely used in simulating the mechanical testing by means of MD simulations [68,69]. To further investigate the mechanical toughness of PNCs, the triaxial tensile test was performed by stretching the periodic box along the X direction at a tensile rate of $\varepsilon = 0.0327/\tau$ while the box length was unchanged in the other two direction. The stress was represented by the deviatoric part of the stress tensor, $\sigma = -P_{XX}$, and the triaxial stress-strain curve can be integrated to obtain the dissipated work with the aim to compare the
mechanical toughening [64,70]. Furthermore, the cyclic
=
tension-recovery and the oscillatory shear deformation were adopted to capture the viscoelastic properties of PNCs. The strain rate of the cyclic tension-recovery deformation was same as the uniaxial tension specified as $\varepsilon = 0.0327/\tau$, and more details can be referred to our previous work [71]. In the cyclic shear deformation, the XY plane of the simulation box was shifted along the X direction. The shear strain was characterized by a sinusoidal function $\gamma_{xy} = \gamma_0 \sin(2\pi\nu t)$. In our simulation, the shear frequency ν was set as $0.01\tau^{-1}$ and the shear strain amplitude γ_0 ranged from 0.05 to 0.5. The shear stress σ_s was described by a sinusoidal
function $\sigma_{xy}(t) = \sigma_0 \sin(2\pi\nu t + \delta) = \sigma' \sin(2\pi\nu t) + \sigma'' \cos(2\pi\nu t)$, where σ_0
is the stress amplitude and δ is the loss angle. The storage modulus G' and loss modulus G'' are derived from the σ' and σ'' parameters with $G' = \sigma'/\gamma_0$, $G'' = \sigma''/\gamma_0$ and $\tan\delta = G''/G' = \sigma''/\sigma'$. All MD runs were carried out by using the large-scale atomic/molecular massively parallel simulator
(LAMMPS) software developed by the Sandia National Laboratories. More simulation details can be found in our previous work [53,54].

2.2. Experimental section

Detailed experimental descriptions are listed in the supporting information.

3. Results and discussion

3.1. Structural properties

Better understanding the structure-property relationship is of fundamental importance in the design and fabrication of all-polymer nanocomposites. Prior to investigating the mechanical and viscoelastic properties, the effect of the degree of intramolecular cross-linking of SCNPs on the structural properties of SCNPs, matrix chains, and the interpenetration in the interface of SCNPs with the matrix chains were investigated. Results on the unfilled system also presented as a reference. The shape and size of SCNPs for each degree of cross-linking were analyzed firstly. As discussed by Moreno et al. [66], shapes of SCNPs are distinct topologies (from the most globular to the sparsest one) even if they are synthesized using the same precursor (same chemistry, mo- lecular weight and fraction of reactive groups). As observed from the snapshots (Fig. 1a), the SCNPs are roughly spheroidal in shape and independently dispersed in the matrix chains. The dispersion state and morphology of SCNPs in the polymer matrix have been characterized by transmission electron microscopy (TEM), as shown in Fig. 1f-i. Many empty areas and areas containing aggregates of nanoparticles can be seen (Fig. 1f, h), which indicates that impenetrable the SiO_2 nano- particles are not uniformly dispersed in the SBR matrix. In contrast, the empty areas decrease in the Fig. 1g, which demonstrates that soft nanoparticles of PS are homogeneously dispersed in the SBR matrix. Furthermore, a good dispersion of soft SBR NPs is shown in the SBR NP/linear SBR blends. The morphology of SBR NPs is nearly spherical (Fig. 1i). The phase behavior of the unfilled styrene-butadiene rubber (SBR) has been studied by using the peak force quantitative nano- mechanical mapping (PF-QNM) mode of the atom force microscope (AFM). The AFM results show that the unfilled SBR is homogeneous, and there are small regional variations in the modulus (Fig. S5), which in- dicates that phase separation has not occurred.

To further confirm the shape of the SCNPs in our simulations, the asphericity A was used to characterize the shape and is defined as:

$$A \quad \frac{\left\langle (\lambda_2 - \lambda_1)^2 + (\lambda_3 - \lambda_1)^2 + (\lambda_3 - \lambda_2)^2 \right\rangle}{2(\lambda_1 + \lambda_2 + \lambda_3)^2} \quad (5)$$

where λ_1, λ_2 and λ_3 is the eigenvalues of the radius of gyration tensor. The possible value of A ranges from 0 to 1. $A = 0$ indicates a spherical shape with $\lambda_1 = \lambda_2 = \lambda_3$, whereas $A = 1$ means a rod-like shape with $\lambda_2 = \lambda_3 = 0$. Table S4 shows the mean asphericity for all investigated systems. The asphericity of SCNPs shows no clear trend, maintaining a value of ~0.185 for all degrees of intramolecular cross-linking, indi- cating that these shapes of SCNPs in our simulations are globular el- lipsoids. The sizes of the SCNPs were characterized using the average
radius of gyration, $\langle R_g^2 \rangle^{1/2}$

$$R_g^2 = \frac{1}{N}\sum_{i=1}^{N}(\mathbf{r}_i - \mathbf{r}_{cm})^2 \quad (6)$$

2.3. Characterization

Details on sample characterization can be found in the supporting information.

where $\mathbf{r}_i$ and $\mathbf{r}_{cm}$ are the position vectors of monomer i in a given chain and the center of the mass of this chain, respectively. To investigate the influence of the matrix chains on the size of SCNPs in detail, we also calculated the particle size of isolated SCNP without any matrix chains (called single SCNP) for each degree of intramolecular cross-linking. Fig. 1b shows that there is no clear variation for the size of single SCNPs as the degree of cross-linking increases in the absence of neigh- boring matrix chains. This indicates that the intramolecular cross- linking does not change the equilibrium dimension of the SCNP in vacuum, in good agreement with the results of Silberstein et al. [72] However, the size of soft SCNPs in PNCs shows a dependence on the degree of cross-linking, decreased with increasing the degree of intra- molecular cross-linking. In addition, the size of soft SCNPs in PNCs is larger than that of single SCNP in vacuum, as well as that of rigid NPs,

indicating that the soft SCNPs are swollen in the PNCs. The origins of these characteristics are two-fold. First, the non-bonded interactions between SCNPs and matrix chains are attractive, mimicking good solvent conditions for all species, compared to vacuum that is analogous to a poor solvent [66,73–75]. Second, the SCNPs are soft and penetrable, indicating that the matrix chains can penetrate into the SCNPs. This in turn leads to a swelling of the SCNPs. The characteristics of the matrix chains were assessed by calculating their radius of gyration $\langle R_g^2 \rangle^{1/2}$ and end-to-end distances $\langle R_{ee}^2 \rangle^{1/2}$

$$R_{ee}^2 = \sum_{i=}^{N-1} \sum_{j=} \mathbf{b}_i \mathbf{b}_j \quad (7)$$

where $\mathbf{b}_i = \mathbf{r}_{i+1} - \mathbf{r}_i$ is the bond vector between the chain beads i and $i+1$. Fig. 1c shows that the present of SCNPs decreases the dimension of polymer chains, in comparison to the unfilled polymer melt, particularly for the $\langle R_{ee}^2 \rangle^{1/2}$ of chains, which is consistent with other simulations [76]. There is almost no effect on the chain dimension for the filled systems as the degree of cross-linking of the SCNPs increases. However, the dimension of polymer chains slightly decreases by increasing the concentration of the nanoparticles due to the confinement effects (Fig. S6), especially at high nanoparticle loadings. In all our simulated systems, the average radius of gyration of matrix chains is equivalent to that of SCNPs.

As mentioned above, the soft and deformable SCNPs can be penetrated by the matrix chains meaning that NPs are wetted by the matrix. Fig. S7 shows the radial distribution function (RDF) of monomers between the SCNPs and matrix chains which gives the indication of the extent of contact. It can be seen that peaks at $r = 1\sigma$, 2σ and 3σ are seen for all systems, where the peak values gradually decrease as the degree of cross-linking increases with the PNCs of the rigid NPs having the lowest value. Such a decrease implies that the contact between matrix chains and SCNPs is reduced. This is not surprising since the rigid NPs are impenetrable and only contact the matrix chains on their surface. To further quantify the degree of penetration of the SCNPs by the matrix chains, the RDF between the center-of-mass of SCNP and the monomers of the matrix chains are shown in Fig. 1d. It can be seen that monomers of matrix chains are located near the center-of-mass of soft SCNPs, demonstrating that the SCNPs are indeed penetrated by the matrix chains. In addition, the degree of penetration of the SCNPs is reduced with increasing the degree of cross-linking, primarily due to the more compact internal structure of SCNPs for the higher degree of cross- linking, resulting in a reduction in the dimension of SCNPs (Fig. 1b). Different from the soft SCNPs in PNCs, the monomers of the matrix chains seem not to appear close to the center of the rigid NPs but at the distance of 0.6 times the radius of the NPs. This implies that there is no penetration into the rigid NPs. It should be noted that the surface of the rigid NPs is rough rather than smooth. In this case, the monomers of matrix chains may begin to be seen within the radius of NPs.

The non-bonded interaction energy between the polymer beads provides configurational information for the degree of folding of SCNPs or the extent of contact between SCNPs and matrix chains. The smaller the value of non-bonded energy (higher absolute value), the stronger the interaction between polymer beads. The intramolecular interaction en- ergy of SCNPs was calculated as shown in Fig. 1e. At equilibrium, for degrees of cross-linking from 10% to 50%, the intramolecular interac- tion energy gradually increases, indicating that the assembly of SCNPs densifies with increasing degree of cross-linking. However, it is increasingly difficult for the matrix chains to penetrate the SCNPs at higher cross-linking density, leading to lower intermolecular interaction energies between the matrix chains and SCNPs (Fig. 1e), especially for rigid NPs. Moreover, the rigid NPs can not be interpenetrated and only contact with the matrix chains on their surface.

3.2. Mechanical properties

3.2.1. Uniaxial tension

After a quantitative study on the influence of the degree of intramolecular cross-linking on the structure of all-polymer nanocomposites, the mechanical properties were examined. Stress-strain curves under uniaxial tension are shown in Fig. 2a. The tensile stress of the all- polymer nanocomposites is higher than that of unfilled system at the same strain, indicating better mechanical reinforcement. Furthermore, the system with rigid NPs has the highest tensile stress compared to the systems of soft SCNPs at the same strain. This indicates that the hard NPs more effectively enhance the mechanical properties than the soft SCNPs.

initially increases with the degree of cross-linking and then tends to decrease at higher degree of cross-linking of the SCNPs. The corresponding tensile stresses at elongation of 300%, 400% and 500% were plotted as a function of the degree of cross-linking in Fig. 2b. It can be seen that there is an optimal degree of intramolecular cross-linking (~30%), where the balance between intra- and intermolecular interactions yield optimal mechanical properties. This phenomenon also occurs in the PNCs with increasing chain length of soft SCNPs (Fig. S8), suggesting that the optimal mechanical enhancement exists regardless of the composition of SCNPs chain length.

The mechanical behavior of all-polymer nanocomposites for four different degrees of intramolecular cross-linking are only briefly described due to the limitation of modeling, computing time and computing resources of the MD simulation. Machine learning algorithms can establish a relationship between the influencing factors and mechanical performance (based on the limited MD simulation data) so as to predict the material properties. To obtain the mechanical properties of the all-polymer nanocomposites with more degrees of intramolecular cross-linking of the SCNPs, the tensile stresses at an elongation of 300% with degrees of cross-linking of the SCNPs equal to 10%, 20%, 30% and 50% were selected as the data sample. First, the Gaussian process (GP) was adopted to complete data augmentation. This process is modeled by infinite-dimensional multivariable Gaussian distribution, and 4 sets of MD data are input to train the GP model. By constructing a GP regression model, 50 sets of tensile stress data at different degrees of cross-linking in the range (10%, 50%) can be obtained, as shown in Fig. 2c.

Next, the data obtained by the GP was applied to train and test the Back Propagation (BP) neural network. Using the generalization of BP neural network, we tried to obtain a more accurate model. The BP neural network has an input layer, a hidden layer, and an output layer. The hidden layer contains 5 nodes. The BP neural network is trained through 40 sets of data, and the remaining 10 are used for testing. Finally, a BP neural network model of the mapping relationship between the degree of cross-linking and tensile stress of 300% strain was obtained. Using the trained model, 200 points are selected for a range of degrees of cross- linking (10% and 50%) to predict a stress at 300% strain. The pre- dicted values are shown in Fig. 2d. We then calculated the tensile stress at 300% strain when the degree of cross-linking was 25% and 45% by MD simulation, to evaluate the accuracy of BP neural network predic- tion results. As shown in Fig. 2d, the results of MD simulation agree well with the BP prediction, which indicates that BP neural network model can accurately predict material properties. This provides a new scheme for predicting the structure-performance relationship and greatly shortens the research and development time. Furthermore, material properties can be obtained in a shorter period of time.

The change in the mechanical strength and the interface with the matrix as the degree of cross-linking of the SCNPs is a consequence of the intra- and intermolecular interactions. The structural evolution of SCNPs was first investigated during the uniaxial deformation to under- stand the origin of the mechanical response of the PNCs. Fig. 3c-e show snapshots of SCNPs and matrix chains at different tensile strains for degree of intramolecular cross-linking of 10% and 50% and for rigid NPs during the tensile process. For clarity, only one SCNP was highlighted in

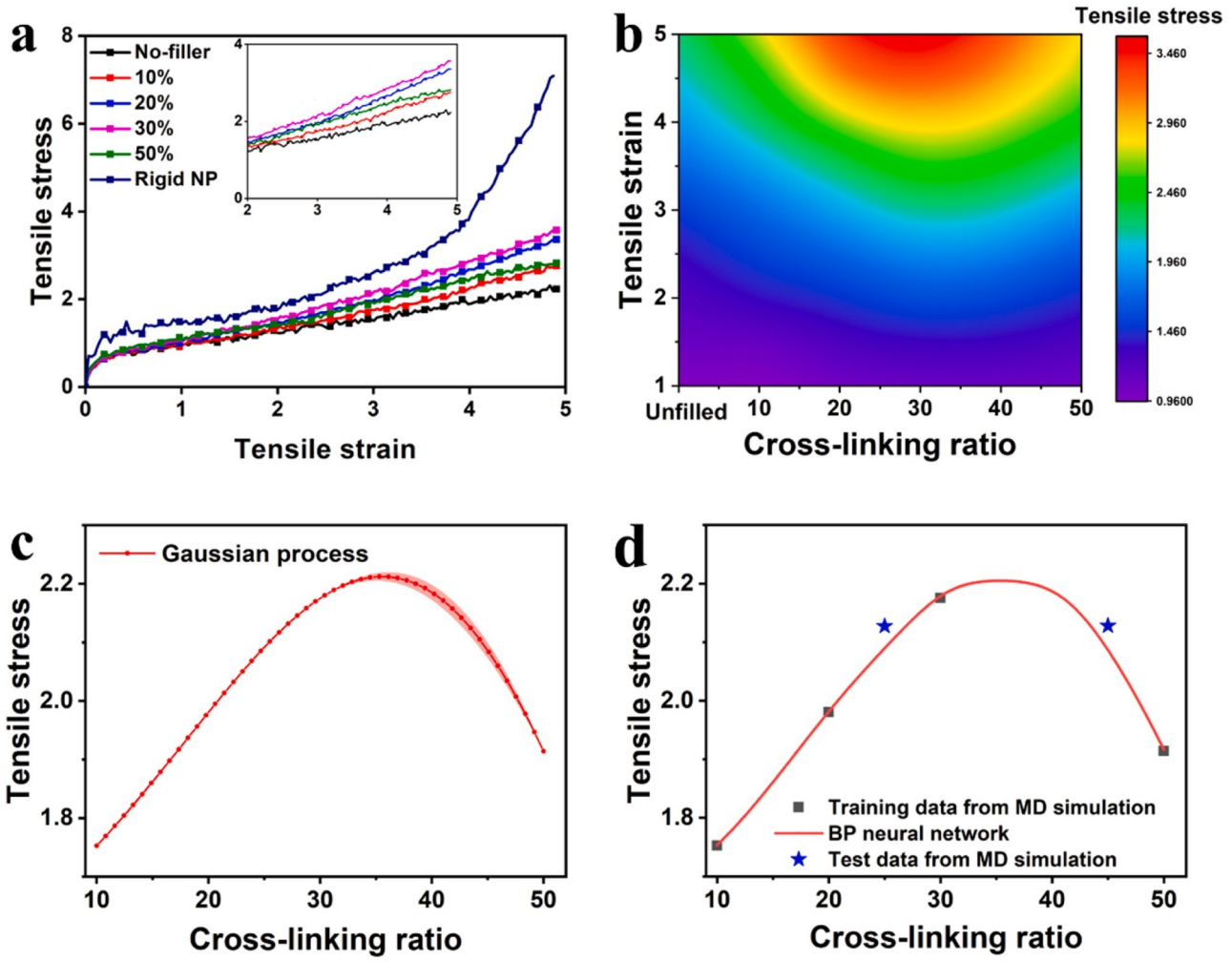

Fig. 2. (a) Tensile stress-strain curves are influenced by the degree of intramolecular cross-linking. (b) Tensile stress as a function of elongation and degree of intra- chain cross-linking. (c) 50 sets of tensile stress data at 300% strain under different degrees of cross-linking obtained by Gaussian process. (d) Tensile stress of 300% strain obtained by MD simulation and predicted by BP neural network.

the snapshots. It can be seen that the SCNPs undergo significant extension in the stretching direction, with the shape of SCNPs changing from globular to ellipsoidal. Their internal structures are pulled apart rather than destroyed due to the restriction of the intramolecular cross-linking. With an increase of the degree of intramolecular cross-linking, the re- striction effect becomes gradually pronounced, hence the extent to which the SCNPs are pulled apart decreases. The rigid NPs show no deformation. To quantitatively interpret these results, we calculated the mean-square radii of gyration tensors of SCNPs along axes parallel and perpendicular to the stretching direction of $R^2_{g,//}$ and $R^2_{g,\perp}$ respectively, normalized by the mean-square radii of gyration tensors of SCNPs under the initial state without stretching (Fig. 3a). $R^2_{g,//}$ monotonically in- creases with the tensile strain at various degrees of cross-linking implying the steady extension of SCNPs along the deformation direction, whereas the $R^2_{g,\perp}$ monotonically decreases with the tensile strain meaning the compression of SCNPs in the perpendicular direction of stretching. Furthermore, $R^2_{g,//}$ is reduced as the degree of cross-linking increases under the same strain, accompanied by an increase in $R^2_{g,\perp}$, showing that it is difficult to stretch or compress the SCNPs that are highly cross-linked. This infers that, as the degree of cross-linking increases, the chain segments are brought closer, decreasing the size of SCNPs, producing more compact SCNPs and increasing the intra- increase in the degree of cross-linking. However, a higher degree of cross-linking decreases the extent of interpenetration between the SCNPs and matrix chains, resulting in a weaker intermolecular interaction, which is deleterious for the mechanical strength of PNCs. This also accounts for the tensile stress decreases of PNCs at high degree of cross-linking (50%). It should be noted that, if the SCNPs are sufficiently rigid, they will neither deform nor interpenetrate with the matrix, i.e., they can be considered as hard NPs, thus weakening intermolecular interaction is not dominant for mechanical strength.

The non-bonded interaction energy was also explored to further molecular interaction of SCNPs. This makes the SCNPs stiffer. Correspondingly, the mechanical enhancement of PNCs also increases with an

understand the molecule mechanism of deformation (Fig. 3b). The intramolecular interactions of SCNPs gradually decreases with the application of tensile strain, indicating that the inner chain segments of SCNPs are pulled apart during stretching. Similar to the equilibrium state, the higher degree of cross-linking of SCNPs produces stronger intramolecular interaction energies at the same tensile strain. Interest- ingly, the interaction energy between the SCNPs and matrix chains monotonically increases for the all-polymer nanocomposites during deformation due to the increase in contact between the SCNPs and matrix chains arising from the deformation of soft SCNPs. In contrast, the interaction energy between the rigid NPs and matrix chains de- creases for the conventional PNCs, implying that a phase separation underpins the material failure. The soft SCNPs may toughen the com- posites and improve their fatigue resistance.

To further reveal the microstructure evolution, the bond orientation

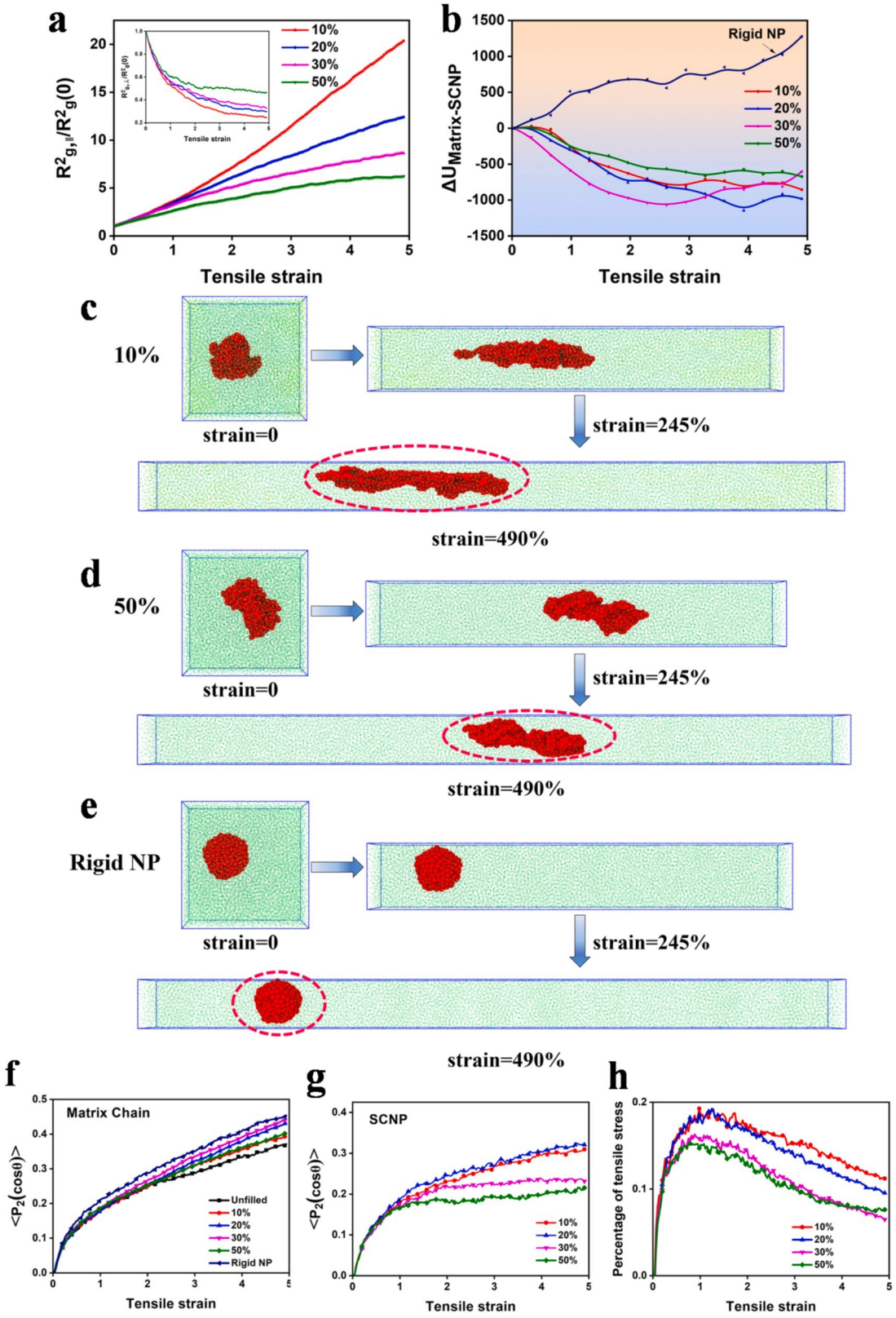

Fig. 3. (a) Radii of gyration of SCNPs along axes parallel and perpendicular (inset) to the stretching direction, normalized by the radii of gyration tensors of SCNPs under the initial state without stretching. (b) Change of the inter-molecular non-bonded interaction energy between matrix chains and SCNPs during the tension process for different degrees of cross-linking of SCNPs. Snapshots of SCNPs and matrix chains for the degree of intra-chain cross-linking of (c) 10%, (d) 50%and (e) rigid NP at different tensile strains during the tensile process. In the interest of clarity, only one SCNP is displayed by red color. Other SCNPs and matrix chains are displayed by green color. Effect of degree of intramolecular cross-linking on the bond orientation behavior of (f) matrix chains and (g) SCNP, and (h) the contribution of SCNPs to the total tensile stress in the process of stretching.

of SCNPs and matrix chains along the stretching direction were also probed (Fig. 3f, g). The bond orientation was measured by the second-order Legendre polynomial:

$$P_2 = \frac{1}{2}\left(3\langle\cos^2\theta\rangle - 1\right) \quad (8)$$

where θ is the angle between the given bond and stretching direction. The bond orientation varies from a perfect orientation normal to the stretching direction ($P_2 = -0.5$), to completely random ($P_2 = 0$) to perfectly aligned in the stretching direction ($P_2 = 1$). During stretching, the bond orientation of the matrix chains in the PNCs is higher than that of unfilled system, imparting better mechanical strength to the PNCs (Fig. 2a). The bond orientation of the matrix chains for conventional PNCs is higher than that of all-polymer nanocomposites. The possible
origin is that, since there is no interpenetration between matrix chains and rigid NPs, the matrix chains can slide on the surface of NPs, producing bridges between rigid NPs, increasing the bond orientation of matrix chains. As a result, conventional PNCs with rigid NPs have the highest tensile stress for a given strain. Additionally, the bond orientation of the matrix chains for all-polymer nanocomposites increases at first and then decreases as the degree of cross-linking increases, with 30% having the highest bond orientation. This is keeping with the results of the mechanical strength. The bond orientation of soft SCNPs, gradually increases with increasing strain. The increasing rate in the orientation of SCNPs for lower degree cross-linking (10% and 20%) greater than that of SCNPs with higher degree of cross-linking (30% and 50%) at larger strains and there is no evident difference at smaller strains. Because of such a lower orientation of SCNPs at high degree of cross-linking at larger strains, it is expected that there will be a reduction in the contribution of SCNPs to the mechanical strength.

The total tensile stress was further analyzed to understand the contribution of each component (Fig. S9). The matrix chains bear the highest external force at a 30% degree of cross-linking due to the bond orientation of matrix chains, in agreement with the results of the mechanical strength. As for the SCNPs, the tensile stress of highly cross-linked SCNPs (30% and 50%) is lower than that of low cross-linked SCNPs (10% and 20%) under larger strains ($\varepsilon > 2.0$). Combining with the characteristics of SCNPs, it can be concluded that, although increasing the degree of cross-linking of SCNPs can make them more compact and stiff, it will weaken their own external tensile force at larger strains during stretching. To further analyze the contribution of SCNPs to the total tensile stress, the percentage of the tensile stress of SCNPs to the total tensile stress was calculated. Fig. 3h shows the contribution of SCNPs to the total tensile stress, which initially increases at $\varepsilon \leq 1.0$ and then decreases with further increasing tensile strain, which can be attributed to the high bond orientation of the matrix chains that bear more of the external force at larger strains and the lower bond orientation of high cross-linked SCNPs.

3.2.2. *Triaxial tension*

In addition to the mechanical strength, the triaxial tension tests were also implemented to examine the mechanical toughness of the PNCs (Fig. S10). At the small strain, all systems show a linear elastic response and then reach apparent yielding point, corresponding to the onset of cavitation. Following the yielding point, the stress continues to decrease attributed to the growth of the cavities. To quantitatively characterize the toughening effect, the triaxial stress-strain curves are integrated to obtain the dissipated work, which gradually increases as a function of the strain. Notably, the all-polymer nanocomposites feature much better toughening than the conventional PNCs and unfilled systems, but their toughening efficiency is slight. Several studies indicated that NP-matrix interfacial interactions were key factors to achieve both a high tough- ening efficiency [70,77,78] and low hysteresis [52] for PNCs. Therefore, the influence of the interfacial adhesion on the mechanical toughness was further investigated by regulating the interaction strength ε_{np}

between the SCNPs and matrix (in Eq. 1). The stress-strain curves (Fig. 4a, b) and dissipated work (Fig. 4f, g) are shown in Fig. 4. Here, the 30%-SCNP systems were chosen as being representative of the all-polymer nanocomposites by taking advantage of the optimal me- chanical strength. The results show that strong interfacial interaction strength ε_{np} can effectively improve the toughening efficiency of both all-polymer nanocomposites and conventional PNCs. However, exces- sive interface interactions are unfavorable to the toughening effect. Nevertheless, the mechanical toughness of the all-polymer nano- composites exceeds that of the conventional PNCs since the SCNPs are soft and deformable and possess a good toughness. Moreover, the sequential breakage of the internal bond in SCNPs occurs to delay propagation of the crack. The experimental results also demonstrate that, in comparison to the unfilled SBR and the SiO_2-300/SBR blends, the tensile strength and elongation at break of the SBR NP/linear SBR blends are much greater, increasing with increasing the SBR NP content (Fig. S12). The fracture toughness of the samples is shown in Fig. 4c. The SBR NP/linear SBR blends have a fracture toughness that is superior to that of the unfilled SBR and the SiO_2-300/SBR blends. It is noteworthy that there is a superior toughening when PS NPs or SBR NPs are used as fillers in the all-polymer nanocomposites when compared to the unfilled system and the conventional PNCs (Fig. 4c, S12 and S14). Their stress-strain curves of parallel tests are shown in Figs. S11 and S13. Schematic diagrams of sequential breakage in unfilled system and the all-polymer nanocomposites are presented in Fig. 4d and e, respectively.

3.3. Viscoelastic properties

3.3.1. Cyclic uniaxial tension-recovery

As mentioned in the Introduction, a decrease in viscosity reduced the friction of polymer segments in the all-polymer nanocomposites with soft deformable SCNPs. This can significantly impact the viscoelasticity of the all-polymer nanocomposites. Subsequently, the tension-recovery deformation was conducted to examine their dynamic mechanical properties. The stress-strain curves are shown in Fig. 5a where it is seen that the stress in recovery is lower than that in tension, reflecting the viscous nature and loss of energy. There is the substantial residual strain (permanent set) remaining after cyclic tension-recovery. Compared to that of the unfilled system, the residual strain in the all-polymer nano- composites is smaller whereas the conventional PNCs have the largest residual strain. Furthermore, the hysteresis loss was analyzed by inte- grating the stress-strain curve (Fig. S15). The hysteresis losses of the filled systems are higher than those of the unfilled system. The degree of intramolecular cross-linking of SCNPs has a slight effect on the hyster- esis loss in the all-polymer nanocomposites. The conventional PNC has the most hysteresis, which may be attributed to the higher chain extension and interfacial friction. Remarkably, the all-polymer nano- composites show a lower hysteresis than the conventional PNC, due to the improved interfacial bonding of the SCNPs. The bond orientation of the polymer matrix at different distances from the SCNPs center of the mass was characterized to explore the local chain orientation (Fig. 5b, c). The rigid NPs are impenetrable, so no matrix chain is seen at the 2–4σ from the SCNPs center of the mass. In contrast, SCNPs can be penetrated by the matrix chains, which can induce the orientation of matrix chains near the SCNPs center of mass. A gradient of the bond orientation of matrix chains in the vicinity of SCNPs center of the mass is seen. Approaching the SCNPs center of the mass, the bond orientation of the matrix chains increases. The conventional PNCs have more a rapid rate of orientation decline of the matrix chains than the all-polymer nano- composites when matrix chains as a function of distance from the NPs mass center, due to the solid-liquid interface of conventional PNCs. Consequently, SCNPs have a much larger influence on the surrounding matrix chains.

To further reveal the viscoelastic response, a five-cycle tension-recovery test was applied. The stress-strain curves are shown in Fig. S16. The corresponding bond orientation of the matrix chains (Fig. S17) and

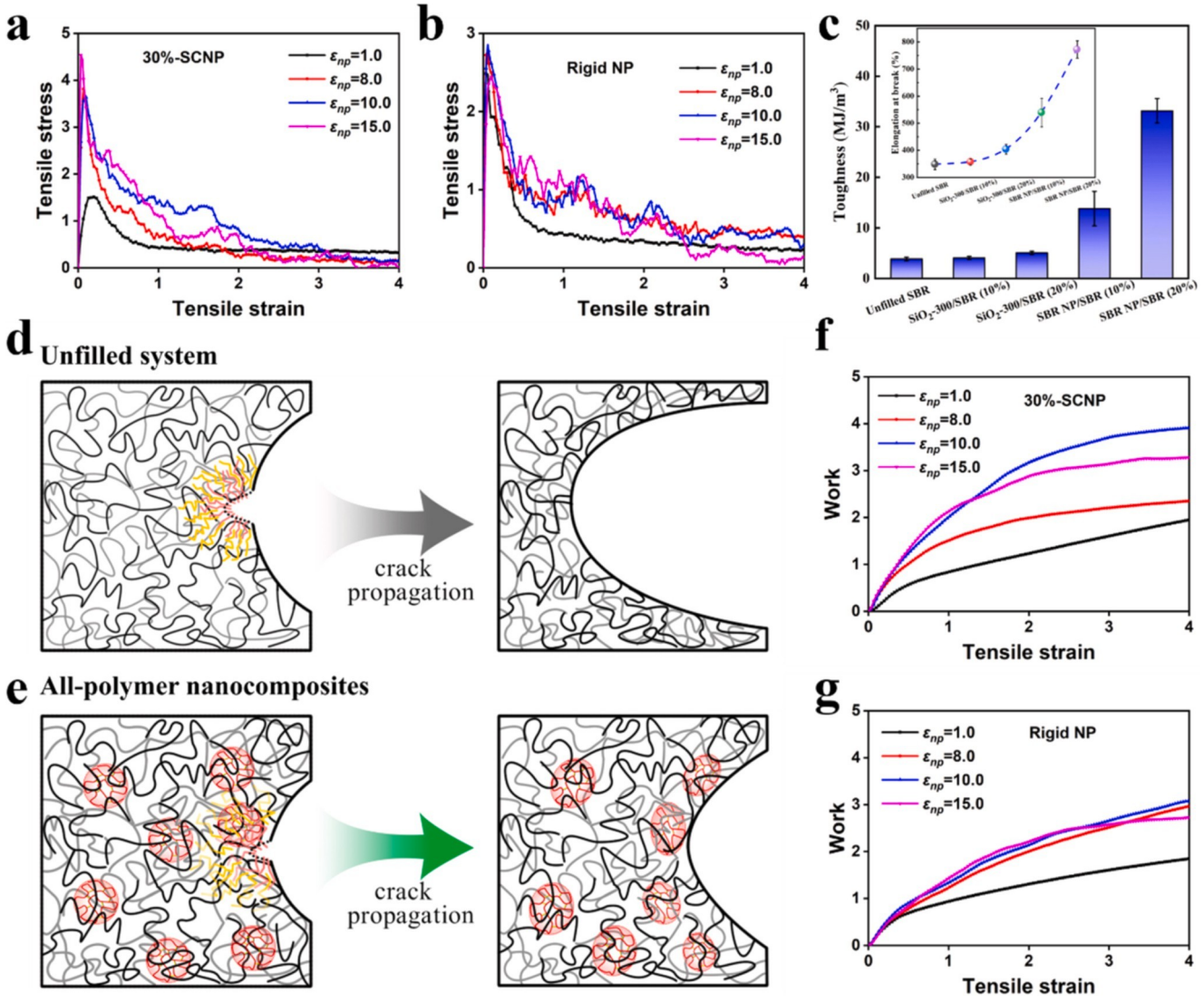

Fig. 4. Effect of the interfacial interaction between SCNPs and matrix chains on the stress-strain curves of (a) the all-polymer nanocomposites with the degree of intramolecular cross-linking of SCNPs equal to 30%, and (b) the conventional PNCs with rigid NPs under the triaxial tensile deformation. (c) Toughness of unfilled SBR, SiO_2-300/SBR and SBR NP/SBR obtained by experiment. Schematic diagram of sequential breakage in (d) unfilled system and (e) the all-polymer nanocomposites. SCNPs are soft and deformable. At the front of a crack, the rupture of the internal bond of SCNPs can delay crack propagation. Dissipated work of (f) the all-polymer nanocomposites with degree of intramolecular cross-linking of SCNPs equal to 30% and (g) the conventional PNCs with rigid NPs, obtained by integrating the stress-strain curves under the triaxial tensile deformation.

SCNPs (Fig. S18) were measured to monitor the morphological change of polymer chains. For a good comparison, the tensile stress and the bond orientation at maximum elongation of 490% as a function of the cycle number are plotted in the Figs. 5e and S19, respectively, indicating a gradual decrease from the first to the fifth loading cycle. At a constant cycle number, the tensile stress and the bond orientation are enhanced in going from the unfilled system to, all-polymer nanocomposites to conventional PNCs. The dynamic mechanical behavior of these systems have similar characteristics, specifically, the tensile stress decreasing at a constant strain with increasing cycle number, especially in the second loading; this is a common phenomenon occurring in elastomers, which is known as the "Mullins effect" (stress softening) [71]. This reduction gradually decreases with the stress-strain curves eventually coinciding with increasing number of cycles. Moreover, the tensile stress of the conventional PNC system drops dramatically (about 60%) from the first to the second cyclic loading, indicating that more variations of the in- ternal structure occur. While the tensile stress of the all-polymer nano- composites and unfilled system only drops moderately.

Similarly, a five-cycle tension-recovery test was also performed on SBR NP/SBR and PS NP/SBR. The stress-strain curves are shown in Figs. S20 and S21. For a better quantitative comparison, the fractional hysteresis loss (%) was also calculated to evaluate the comprehensive properties of the materials, defined by the ratio of the dissipated energy to the stored energy during the tension-recovery process. Experiment and simulations indicate that the all-polymer nanocomposites have remarkably lower hysteresis (%) when compared to traditional PNCs with rigid NPs in each cycle of loading (Figs. S22, S23 and 5g, h). From the above discussion, it can be concluded that the conventional PNCs have a better mechanical enhancement but a much higher hysteresis

loss , whereas the all-polymer nanocomposites can balance the mechanical and viscoelastic properties, i.e., they can not only enhance and toughen the materials, but also bring a low hysteresis. The underlying reasons are that SCNPs can be interpenetrated by the matrix chains resulting in a good interfacial bonding and low interfacial friction. On the other hand, the deformation of SCNPs is reversible. This can drive

the surrounding matrix chains to move, playing an important role in the

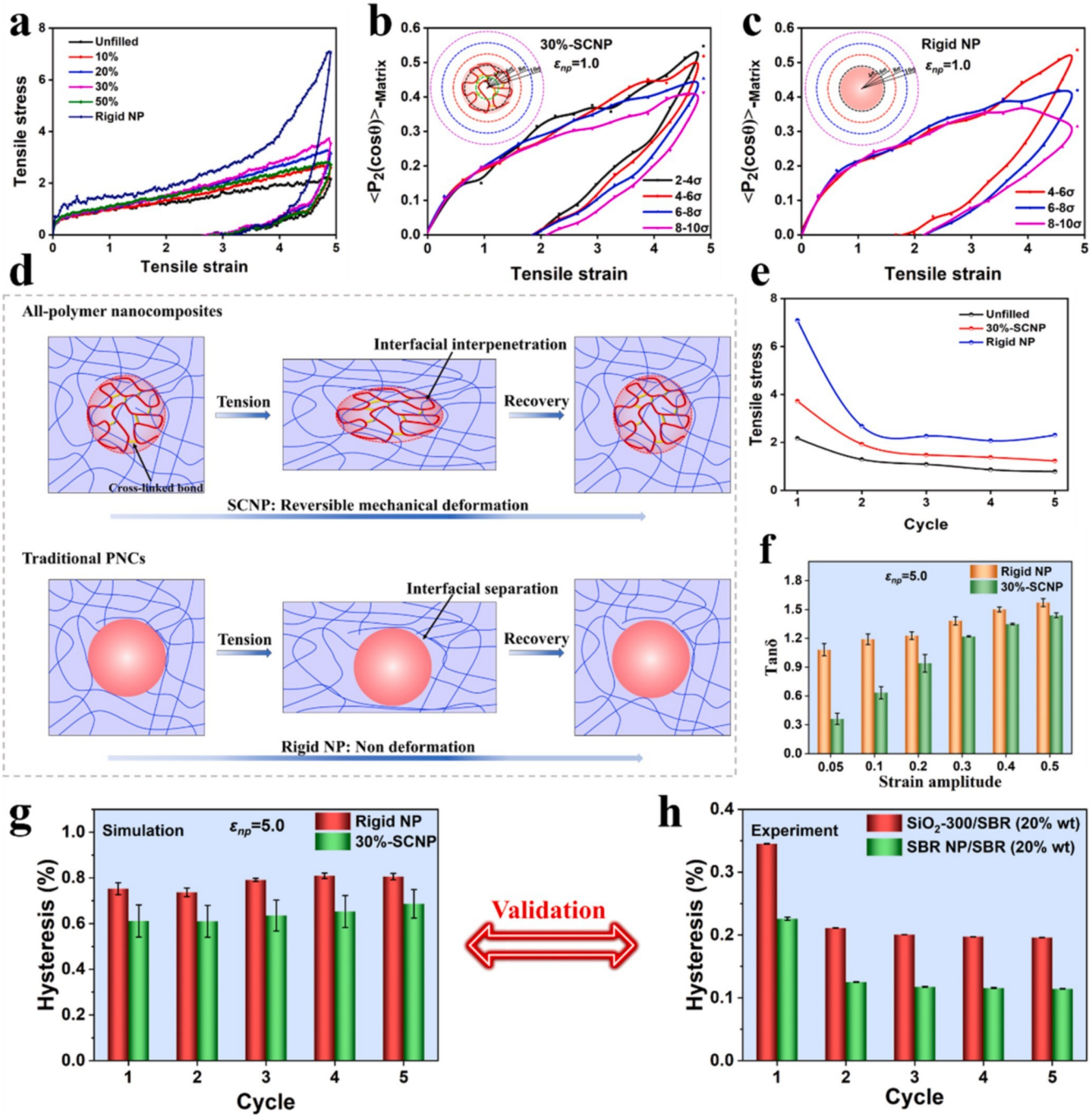

Fig. 5. (a) Tensile loading-unloading curves for different degrees of intramolecular cross-linking of SCNPs. Bond orientation of matrix chain at different distances from the SCNPs center of the mass for (b) 30%-SCNP all-polymer nanocomposites and (c) conventional PNCs under the load-unload. (d) Difference of the microscopic deformation between the all-polymer nanocomposites and the traditional PNCs during the tension-recovery process. (e) Tensile stress as a function of cycle number for these three systems. (f) Tangent loss versus dynamic cyclic shear strain amplitude for the all-polymer nanocomposites and the traditional PNCs with the interfacial interaction between NP and matrix chains $\varepsilon_{np} = 5.0$. The shear frequency is $\omega = 0.01\tau^{-1}$. (g) Hysteresis loss (%) of the all-polymer nanocomposites and the traditional PNCs with $\varepsilon_{np} = 5.0$ under different cycle number. (h) Experimental results of hysteresis energy loss for SBR NP/SBR (20% wt) and SiO_2-300/SBR (20% wt).

energy dissipation. The difference in the microscopic deformation between the all-polymer nanocomposites and the traditional PNCs during the tension-recovery process is shown in Fig. 5d.

3.3.2. *Dynamic shear*

The influence of the nature of the NPs on the dynamic shear behaviors was investigated. The storage modulus G' and the loss modulus G'' as a function of the shear strain amplitude γ_0 at the constant shear frequency of $\omega = 0.01\tau^{-1}$ are shown in Fig. S24a, b to determine the viscoelastic response of the system. The PNCs with the rigid NPs exhibit the highest value of both the storage and loss modulus, and the two moduli decrease markedly with increasing shear strain amplitude, reflecting the most notable non-linear behavior (known as the Payne effect). Such a decrease in modulus at a large strain is due, more than likely, to the disruption of the NP-NP interaction. At low strain ampli-

tudes, the rigid NPs show poorer dispersion and stronger interaction

resulting in a higher storage modulus. As the strain amplitude increases, the direct contact between the NP-NP is greatly reduced, leading to a substantial decrease in NP-NP interactions, which causes a rapid decrease in the storage modulus. However, G' and G'' for the all-polymer nanocomposites with the soft SCNPs as well as the unfilled system exhibit only a very slight change as the strain amplitude increases, resulting in a very weak Payne effect. This can be attributed to the good interfacial bonding between the matrix chains and SCNPs. The PNCs filled with soft SCNPs have higher storage modulus G' and loss modulus G'' than the unfilled system, indicating an enhancement in reinforcement.

The tangent loss was calculated to further explore the energy dissipation of the PNCs (Fig. S24c), which is defined as the ratio of loss modulus to storage modulus ($\tan\delta = G''/G'$). The $\tan\delta$ of the rigid NPs system increases considerably with the strain amplitude, indicating the most significant nonlinearity with the strain. In contrast, $\tan\delta$ of the soft SCNPs systems changes in a relatively moderate manner implying an unremarkable Payne effect. The $\tan\delta$ can serve as a good indicator of the ratio of viscous to the elastic properties. Unexpectedly, the soft SCNPs systems exhibit a lower $\tan\delta$ compared to the rigid NPs systems espe- cially at smaller strain amplitudes, reflecting the lower viscosity and higher elasticity. This phenomenon becomes more significant when the interfacial interaction $\varepsilon_{np} = 5.0$, as shown in Fig. 5f. In combination with G' and G'', this can be explained by their strong interfacial bonding of the soft SCNPs and the matrix chains, that can greatly reduce the energy dissipation arising from interfacial friction. The solid-liquid interface of the rigid NPs system leads to a much greater interfacial friction and the highest loss modulus (Fig. S24b) that gives rise to the highest viscous dissipation.

3.4. Integration of mechanical and viscoelastic properties

As demonstrated previously, the all-polymer nanocomposites comprised of SCNPs and linear matrix chains, leads to a high mechanical strength, toughness and low hysteresis due to the soft interface and its effect on the surrounding matrix chains. The strong interfacial interaction ε_{np} between the SCNPs and matrix can effectively improve the mechanical toughness of the PNCs. However, excessive interfacial interactions are unfavorable to the movement of the polymer chains, which induces a weaker toughening effect. The influence of interfacial adhesion on the mechanical strength and hysteresis (%) was further investigated, and the resultant stress-strain curves are shown in Figs. S25-S26. All results are summarized in the tensile stress-hysteresis diagram (Fig. 6). A strong adhesion ε_{np} effectively improves the me- chanical strength and depresses the dynamical hysteresis of both the all- polymer nanocomposites and conventional PNCs. However, the all- polymer nanocomposites show a better mechanical strength and lower hysteresis than conventional PNCs under the same ε_{np} and cycle number, which is further manifest in the shear deformation (Fig. S27). The all-polymer nanocomposites have a higher G' and lower $\tan\delta$ at the same ε_{np}. The toughness-hysteresis diagram is plotted in Fig. 6. The all-polymer nanocomposites have a higher toughness and lower hysteresis than the unfilled system and conventional PNCs, particularly in the strong interfacial interaction.

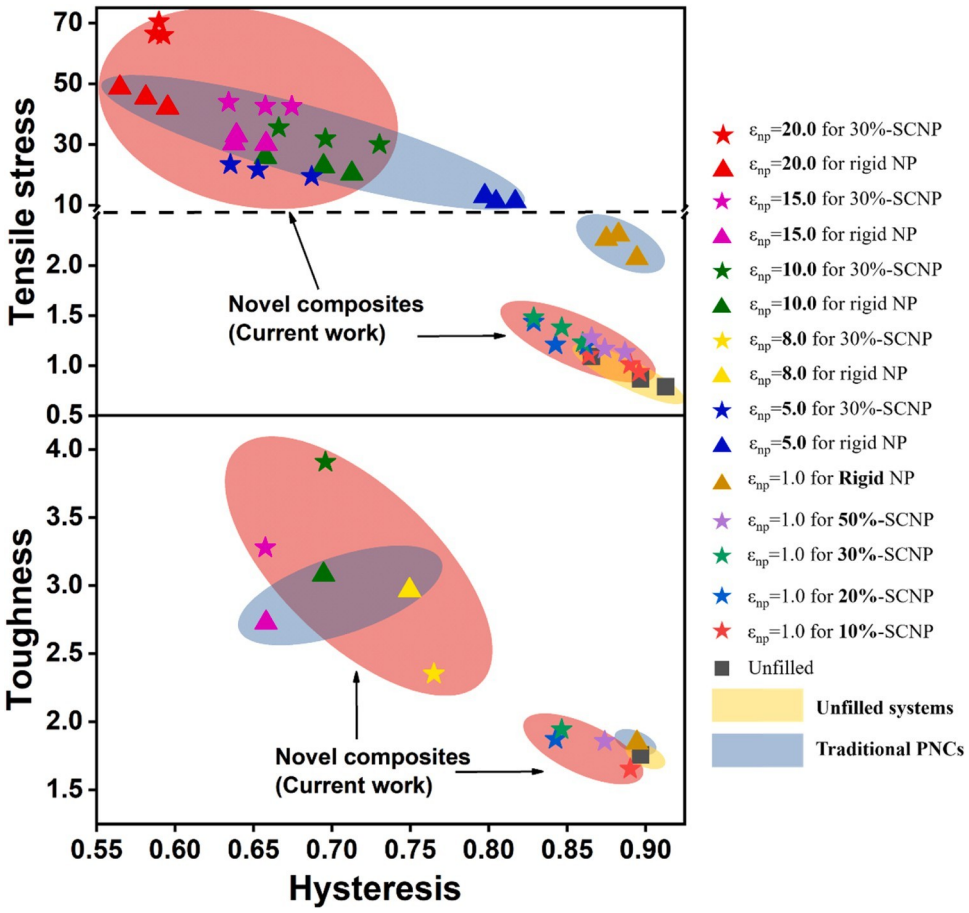

Fig. 6. Tensile stress-hysteresis diagram and toughness-hysteresis diagram. The three identical symbols for one condition represent the third, fourth and fifth tension-recovery, respectively. The tensile stress adopted here is at the elongation of 490%. The hysteresis denotes the ratio of the dissipated energy during the tension-recovery process to the stored energy during the tension process. Toughness was obtained by the integration of the stress-strain curve under the triaxial tensile deformation.

In summary, the SCNPs are incorporated into the polymer matrix chains providing excellent mechanical strength, toughness and low hysteresis, by manipulating the intramolecular cross-linking of the SCNPs and adhesion between the SCNPs and polymer matrix. Such an advantage can be considerably amplified with the proper increase of the interfacial adhesion between the SCNPs and polymer matrix. It should be noted that the hysteresis ranges from 55% to 90% in the current simulations, which appears to be larger than those obtained from ex- periments. This is mainly attributed to the non-crosslinked matrix chains adopted in our simulations so as to better explore the interpenetration effect, since the mobility of the cross-linked polymer matrix chains is significantly restrained and detrimental to penetrate into SCNPs. How- ever, the qualitative comparisons between our results are reasonable.

4. Conclusions

In this work, using a combination of simulation and experimental results, a new "SCNPs effect" balance mechanism is proposed to further advance the practical application of the all-polymer nanocomposites by incorporating single-chain nanoparticles (SCNPs) into linear polymer chains. Using soft, deformable SCNPs instead of rigid NPs not only effectively improves the mechanical properties but depresses the dy- namic hysteresis due to the soft interface and SCNP deformation. The intramolecular cross-linking of the SCNPs and adhesion between the SCNPs and polymer matrix are critical for realizing such high- performance systems. There is an optimal degree of cross-linking of
~30% for the SCNPs to achieve the best mechanical strength via balancing intra- and intermolecular interactions. Based on a Gaussian regression model and back propagation (BP) neural network, the mechanical strength of the all-polymer nanocomposites under various degrees of intramolecular cross-linking of the SCNPs can be predicted and is supported by simulations. Furthermore, the mechanical toughness of the all-polymer nanocomposites is superior to the unfilled system and conventional PNCs especially with stronger interfacial interaction due to the soft character of the SCNPs and the internal bond rupture of the cross-linked SCNPs. Interestingly, the all-polymer nanocomposites exhibit the lowest fractional hysteresis loss than those of the unfilled system and conventional PNCs under cyclic uniaxial tensile deforma- tion. The dynamic shear tests demonstrate that the all-polymer nano- composites show unremarkable non-linear behavior (Payne effect) and lower energy dissipation, whereas the conventional PNCs have the most notable non-linear behavior and higher energy loss. In summary, the all- polymer nanocomposites show unique advantages in balancing the mechanical strength, mechanical toughness and dynamic hysteresis loss simultaneously. This study provides a novel strategy to reconcile the toughness-strength and the toughness-hysteresis dilemmas to capture the versatility of materials, such as elastomers and gels, with their great potential applications in flexible robots, actuators and sensors.

CRediT authorship contribution statement

Haixiao Wan: Methodology, Investigation, Resource, Date curation, Writing - original draft. **Sai Li:** Methodology, Investigation, Resource, Date curation, Writing - original draft. **Yachen Wang:** Investigation, Data curation. **Zhudan Chen:** Software. **Junwei He:** Investigation, Data curation. **Chunhua Li:** Investigation. **Gengxin Liu:** Investigation. **Jun Liu:** Conceptualization, Supervision, Writing - review & editing, Funding acquisition. **Xiaodong Wang:** Supervision. **Thomas P. Rus- sell:** Supervision, Writing - review & editing. **Liqun Zhang:** Supervision.

Declaration of Competing Interest

The authors declare that they have no known competing financial interests or personal relationships that could have appeared to influence the work reported in this paper.

Data availability

Data will be made available on request.

Acknowledgements

H.W. and S.L. contribute equally to this work. This work was financially supported by the National Science Fund for Excellent Young Scholars (52122311), the Major Program (51790502) of the National Natural Science Foundation of China, the National Natural Science Foundation of China (51873006, 21674010 and 51333004), the Beijing Municipal Natural Science Foundation (2182053) and the Fok Ying- Tong Education Foundation of China (Grant No. 171040).

Appendix A. Supporting information

Supplementary data associated with this article can be found in the online version at doi:10.1016/j.nanoen.2023.108925.

References

[1] A.C. Balazs, T. Emrick, T.P. Russell, Nanoparticle polymer composites: Where two small worlds meet, Science 314 (2006) 1107–1110, https://doi.org/10.1126/ science.1130557.

[2] V. Ganesan, A. Jayaraman, Theory and simulation studies of effective interactions, phase behavior and morphology in polymer nanocomposites, Soft Matter 10 (2014) 13–38, https://doi.org/10.1039/c3sm51864g.

[3] R. Krishnamoorti, R.A. Vaia, Polymer nanocomposites, J. Polym. Sci. Pt. B-Polym. Phys. 45 (2007) 3252–3256, https://doi.org/10.1002/polb.21319.

[4] T.D. Zhang, X.W. Zhao, C.H. Zhang, Y. Zhang, Y.Q. Zhang, Y. Feng, Q.G. Chi, Q. G. Chen, Polymer nanocomposites with excellent energy storage performances by utilizing the dielectric properties of inorganic fillers, Chem. Eng. J. 408 (2021), 127314, https://doi.org/10.1016/j.cej.2020.127314.

[5] Y. Zhang, C.H. Zhang, Y. Feng, T.D. Zhang, Q.G. Chen, Q.G. Chi, L.Z. Liu, G.F. Li, Y. Cui, X. Wang, Z.M. Dang, Q.Q. Lei, Excellent energy storage performance and thermal property of polymer-based composite induced by multifunctional one-dimensional nanofibers oriented in-plane direction, Nano Energy 56 (2019) 138–150, https://doi.org/10.1016/j.nanoen.2018.11.044.

[6] K.S. Soppimath, T.M. Aminabhavi, A.R. Kulkarni, W.E. Rudzinski, Biodegradable polymeric nanoparticles as drug delivery devices, J. Control. Release 70 (2001) 1–20, https://doi.org/10.1016/S0168-3659(00)00339-4.

[7] I. Brigger, C. Dubernet, P. Couvreur, Nanoparticles in cancer therapy and diagnosis, Adv. Drug Deliv. Rev. 54 (2002) 631–651, https://doi.org/10.1016/S0169-409x(02)00044-3.

[8] S.K. Lai, D.E. O'Hanlon, S. Harrold, S.T. Man, Y.Y. Wang, R. Cone, J. Hanes, Rapid transport of large polymeric nanoparticles in fresh undiluted human mucus, Proc. Natl. Acad. Sci. 104 (2007) 1482–1487, https://doi.org/10.1073/pnas.0608611104.

[9] K.J. Cho, X. Wang, S.M. Nie, Z. Chen, D.M. Shin, Therapeutic nanoparticles for drug delivery in cancer, Clin. Cancer Res. 14 (2008) 1310–1316, https://doi.org/ 10.1158/1078-0432.CCR-07-1441.

[10] J. Liang, Y. Huang, L. Zhang, Y. Wang, Y. Ma, T. Guo, Y. Chen, Molecular-Level Dispersion of Graphene into Poly(vinyl alcohol) and Effective Reinforcement of their Nanocomposites, Adv. Funct. Mater. 19 (2009) 2297–2302, https://doi.org/ 10.1002/adfm.200801776.

[11] L. Liu, A. Barber, S. Nuriel, D. Wagner, Mechanical properties of functionalized single-walled carbon-nanotube/poly(vinyl alcohol) nanocomposites, Adv. Funct. Mater. 15 (2005) 975–980, https://doi.org/10.1002/adfm.200400525.

[12] N. Domun, H. Hadavinia, T. Zhang, T. Sainsbury, G.H. Liaghat, S. Vahid, Improving the fracture toughness and the strength of epoxy using nanomaterials - a review of the current status, Nanoscale 7 (2015) 10294–10329, https://doi.org/10.1039/ c5nr01354b.

[13] K. Haraguchi, T. Takehisa, Nanocomposite hydrogels: A unique organic-inorganic network structure with extraordinary mechanical, optical, and swelling/de-swelling properties, Adv. Mater. 14 (2002) 1120–1124, https://doi.org/10.1002/ 1521-4095(20020816)14:16<1120::aid-adma1120>3.0.co;2-9.

[14] C. Teng, J. Qiao, J. Wang, L. Jiang, Y. Zhu, Hierarchical layered heterogeneous graphene-poly(n-isopropylacrylamide)-clay hydrogels with superior modulus, strength, and toughness, ACS Nano 10 (2016) 413–420, https://doi.org/10.1021/acsnano.5b05120.

[15] M. Morits, T. Verho, J. Sorvari, V. Liljestro¨m, M.A. Kostiainen, A.H. Gro¨schel, O. Ikkala, Toughness and fracture properties in nacre-mimetic clay/polymer nanocomposites, Adv. Funct. Mater. 27 (2017), 1605378, https://doi.org/10.1002/adfm.201605378.

[16] C. Zhang, Z.J. Yang, N.T. Duong, X.H. Li, Y. Nishiyama, Q. Wu, R.C. Zhang, P. C. Sun, Using dynamic bonds to enhance the mechanical performance: from microscopic molecular interactions to macroscopic properties, Macromolecules 52 (2019) 5014–5025, https://doi.org/10.1021/acs.macromol.9b00503.

[17] X. Zhang, W. Liu, D. Yang, X. Qiu, Biomimetic supertough and strong biodegradable polymeric materials with improved thermal properties and excellent

UV-blocking performance, Adv. Funct. Mater. 29 (2019), 1806912, https://doi.org/10.1002/adfm.201806912.
[18] J. Huang, J. Fan, L. Cao, C. Xu, Y. Chen, A novel strategy to construct co-continuous PLA/NBR thermoplastic vulcanizates: Metal-ligand coordination-induced dynamic vulcanization, balanced stiffness-toughness and shape memory effect, Chem. Eng. J. 385 (2020), 123828, https://doi.org/10.1016/j.cej.2019.123828.
[19] Y. Shi, C. Liu, Z. Duan, B. Yu, M. Liu, P. Song, Interface engineering of MXene towards super-tough and strong polymer nanocomposites with high ductility and excellent fire safety, Chem. Eng. J. 399 (2020), 125829, https://doi.org/10.1016/j.cej.2020.125829.
[20] N. Song, Z. Gao, X. Li, Tailoring nanocomposite interfaces with graphene to achieve high strength and toughness, Sci. Adv. 6 (2020), eaba7016, https://doi.org/10.1126/sciadv.aba7016.
[21] M. Gonzalez-Burgos, A. Latorre-Sanchez, J.A. Pomposo, Advances in single chain technology, Chem. Soc. Rev. 44 (2015) 6122–6142, https://doi.org/10.1039/c5cs00209e.
[22] T. Terashima, T. Mes, T.F.A. De Greef, M.A.J. Gillissen, P. Besenius, A.R. A. Palmans, E.W. Meijer, Single-Chain Folding of Polymers for Catalytic Systems in Water, J. Am. Chem. Soc. 133 (2011) 4742–4745, https://doi.org/10.1021/ja2004494.
[23] J. Rubio-Cervilla, E. Gonzalez, J.A. Pomposo, Advances in single-chain nanoparticles for catalysis applications, Nanomaterials 7 (2017) 341, https://doi.org/10.3390/nano7100341.
[24] H. Rothfuss, N.D. Knofel, P.W. Roesky, C. Barner-Kowollik, Single-chain nanoparticles as catalytic nanoreactors, J. Am. Chem. Soc. 140 (2018) 5875–5881, https://doi.org/10.1021/jacs.8b02135.
[25] C.A. Tooley, S. Pazicni, E.B. Berda, Toward a tunable synthetic [FeFe] hydrogenase mimic: single-chain nanoparticles functionalized with a single diiron cluster, Polym. Chem. 6 (2015) 7646–7651, https://doi.org/10.1039/c5py01196e.
[26] M.A.J. Gillissen, I.K. Voets, E.W. Meijer, A.R.A. Palmans, Single chain polymeric nanoparticles as compartmentalised sensors for metal ions, Polym. Chem. 3 (2012) 3166–3174, https://doi.org/10.1039/c2py20350b.
[27] M.A.J. Gillissen, T. Terashima, E.W. Meijer, A.R.A. Palmans, I.K. Voets, Sticky supramolecular grafts stretch single polymer chains, Macromolecules 46 (2013) 4120–4125, https://doi.org/10.1021/ma4006846.
[28] A. Latorre-Sanchez, J.A. Pomposo, A simple, fast and highly sensitive colorimetric detection of zein in aqueous ethanol via zein-pyridine-gold interactions, Chem. Commun. 51 (2015) 15736–15738, https://doi.org/10.1039/c5cc06083d.
[29] O. Altintas, C. Barner-Kowollik, Single-chain folding of synthetic polymers: a critical update, Macromol. Rapid Commun. 37 (2016) 29–46, https://doi.org/10.1002/marc.201500547.
[30] S.K. Hamilton, E. Harth, Molecular dendritic transporter nanoparticle vectors provide efficient intracellular delivery of peptides, Acs Nano 3 (2009) 402–410, https://doi.org/10.1021/nn800679z.
[31] A. Sanchez-Sanchez, S. Akbari, A.J. Moreno, F.Lo Verso, A. Arbe, J. Colmenero, J. A. Pomposo, Design and preparation of single-chain nanocarriers mimicking disordered proteins for combined delivery of dermal bioactive cargos, Macromol. Rapid Commun. 34 (2013) 1681–1686, https://doi.org/10.1002/marc.201300562.
[32] J. De-La-Cuesta, E. Gonzalez, J.A. Pomposo, Advances in fluorescent single-chain nanoparticles, Molecules 22 (2017) 1819, https://doi.org/10.3390/molecules22111819.
[33] A.P.P. Kroger, J.M.J. Paulusse, Single-chain polymer nanoparticles in controlled drug delivery and targeted imaging, J. Control. Release 286 (2018) 326–347, https://doi.org/10.1016/j.jconrel.2018.07.041.
[34] E.M. Harth, S. Hecht, B. Helms, E.E. Malmstrom, J.M.J. Frechet, C.J. Hawker, The effect of macromolecular architecture in nanomaterials: A comparison of site isolation in porphyrin core dendrimers and their isomeric linear analogues, J. Am. Chem. Soc. 124 (2002) 3926–3938, https://doi.org/10.1021/ja025536u.
[35] A.E. Cherian, F.C. Sun, S.S. Sheiko, G.W. Coates, Formation of nanoparticles by intramolecular cross-linking: Following the reaction progress of single polymer chains by atomic force microscopy, J. Am. Chem. Soc. 129 (2007) 11350, https:// doi.org/10.1021/ja0743011.
[36] C.K. Lyon, A. Prasher, A.M. Hanlon, B.T. Tuten, C.A. Tooley, P.G. Frank, E. B. Berda, A brief user's guide to single-chain nanoparticles, Polym. Chem. 6 (2015) 181–197, https://doi.org/10.1039/c4py01217h.
[37] S. Mavila, O. Eivgi, I. Berkovich, N.G. Lemcoff, Intramolecular cross-linking methodologies for the synthesis of polymer nanoparticles, Chem. Rev. 116 (2016) 878–961, https://doi.org/10.1021/acs.chemrev.5b00290.
[38] J.T. Luo, Y.H. Zhu, Y.F. Ruan, W.W. Wu, X.K. Ouyang, Z.K. Du, G.X. Liu, Diameter and elasticity governing the relaxation of soft-nanoparticle melts, Macromolecules 54 (2021) 8077–8087, https://doi.org/10.1021/acs.macromol.1c01111.
[39] A.J. Moreno, F. Lo Verso, A. Sanchez-Sanchez, A. Arbe, J. Colmenero, J. A. Pomposo, Advantages of orthogonal folding of single polymer chains to soft nanoparticles, Macromolecules 46 (2013) 9748–9759, https://doi.org/10.1021/ma4021399.
[40] A.M. Hanlon, R.W. Chen, K.J. Rodriguez, C. Willis, J.G. Dickinson, M. Cashman, E. B. Berda, Scalable synthesis of single-chain nanoparticles under mild conditions, Macromolecules 50 (2017) 2996–3003, https://doi.org/10.1021/acs.macromol.7b00497.
[41] A. Levy, R. Feinstein, C.E. Diesendruck, Mechanical unfolding and thermal refolding of single-chain nanoparticles using ligand-metal bonds, J. Am. Chem. Soc. 141 (2019) 7256–7260, https://doi.org/10.1021/jacs.9b01960.

[42] M.E. Mackay, T.T. Dao, A. Tuteja, D.L. Ho, B. Van Horn, H.C. Kim, C.J. Hawker, Nanoscale effects leading to non-Einstein-like decrease in viscosity, Nat. Mater. 2 (2003) 762–766, https://doi.org/10.1038/nmat999.
[43] M.E. Mackay, A. Tuteja, P.M. Duxbury, C.J. Hawker, B. Van Horn, Z.B. Guan, G. H. Chen, R.S. Krishnan, General strategies for nanoparticle dispersion, Science 311 (2006) 1740–1743, https://doi.org/10.1126/science.1122225.
[44] A. Tuteja, M.E. Mackay, C.J. Hawker, B. Van Horn, Effect of ideal, organic nanoparticles on the flow properties of linear polymers: Non-Einstein-like behavior, Macromolecules 38 (2005) 8000–8011, https://doi.org/10.1021/ ma050974h.
[45] A. Tuteja, P.M. Duxbury, M.E. Mackay, Polymer chain swelling induced by dispersed nanoparticles, Phys. Rev. Lett. 100 (2008), 077801, https://doi.org/10.1103/PhysRevLett.100.077801.
[46] T. Chen, H.Y. Zhao, R. Shi, W.F. Lin, X.M. Jia, H.J. Qian, Z.Y. Lu, X.X. Zhang, Y. K. Li, Z.Y. Sun, An unexpected N-dependence in the viscosity reduction in all- polymer nanocomposite, Nat. Commun. 10 (2019), 5552, https://doi.org/ 10.1038/s41467-019-13410-z.
[47] T. Chen, H.J. Qian, Y.L. Zhu, Z.Y. Lu, Structure and dynamics properties at interphase region in the composite of polystyrene and cross-linked polystyrene soft nanoparticle, Macromolecules 48 (2015) 2751–2760, https://doi.org/10.1021/ ma502383n.
[48] T. Chen, H.J. Qian, Z.Y. Lu, Diffusion dynamics of nanoparticle and its coupling with polymers in polymer nanocomposites, Chem. Phys. Lett. 687 (2017) 96–100, https://doi.org/10.1016/j.cplett.2017.09.010.
[49] T. Chen, H.J. Qian, Z.Y. Lu, Note: Chain length dependent nanoparticle diffusion in polymer melt: Effect of nanoparticle softness, J. Chem. Phys. 145 (2016), 106101, https://doi.org/10.1063/1.4962370.
[50] X.-M. Jia, R. Shi, G.-S. Jiao, T. Chen, H.-J. Qian, Z.-Y. Lu, Temperature effect on interfacial structure and dynamics properties in polymer/single-chain nanoparticle composite, Macromol. Chem. Phys. 218 (2017), 1700029, https://doi.org/ 10.1002/macp.201700029.
[51] P. Ba˘cova´, F. Lo Verso, A. Arbe, J. Colmenero, J.A. Pomposo, A.J. Moreno, The role
of the topological constraints in the chain dynamics in all-polymer nanocomposites, Macromolecules 50 (2017) 1719–1731, https://doi.org/10.1021/ acs.macromol.6b02340.
[52] Z.J. Wang, C.P. Xiang, X. Yao, P. Le Floch, J. Mendez, Z.G. Suo, Stretchable materials of high toughness and low hysteresis, Proc. Natl. Acad. Sci. 116 (2019) 5967–5972, https://doi.org/10.1073/pnas.1821420116.
[53] J. Liu, Z.J. Zheng, F.Z. Li, W.W. Lei, Y.Y. Gao, Y.P. Wu, L.Q. Zhang, Z.L. Wang, Nanoparticle chemically end-linking elastomer network with super-low hysteresis loss for fuel-saving automobile, Nano Energy 28 (2016) 87–96, https://doi.org/ 10.1016/j.nanoen.2016.08.002.
[54] J. Liu, Y.L. Lu, M. Tian, F. Li, J.X. Shen, Y.Y. Gao, L.Q. Zhang, The interesting influence of nanosprings on the viscoelasticity of elastomeric polymer materials: simulation and experiment, Adv. Funct. Mater. 23 (2013) 1156–1163, https://doi.org/10.1002/adfm.201201438.
[55] K. Kremer, G.S. Grest, Dynamics of entangled linear polymer melts: A molecular- dynamics simulation, J. Chem. Phys. 92 (1990) 5057–5086, https://doi.org/ 10.1063/1.458541.
[56] D. Reith, H. Meyer, F. Müller-Plathe, Mapping atomistic to coarse-grained polymer models using automatic simplex optimization to fit structural properties, Macromolecules 34 (2001) 2335–2345, https://doi.org/10.1021/ma001499k.
[57] H. Fukunaga, T. Aoyagi, J.-i Takimoto, M. Doi, Derivation of coarse-grained potential for polyethylene, Comput. Phys. Commun. 142 (2001) 224–226, https:// doi.org/10.1016/s0010-4655(01)00311-3.
[58] L.J. Chen, H.J. Qian, Z.Y. Lu, Z.S. Li, C.C. Sun, An automatic coarse-graining and fine-graining simulation method: application on polyethylene, J. Phys. Chem. B 110 (2006) 24093–24100, https://doi.org/10.1021/jp0644558.
[59] D. Curco´, C. Alem´an, Coarse-grained simulations of amorphous and melted polyethylene, Chem. Phys. Lett. 436 (2007) 189–193, https://doi.org/10.1016/j.cplett.2007.01.031.
[60] E. Panizon, D. Bochicchio, L. Monticelli, G. Rossi, MARTINI coarse-grained models of polyethylene and polypropylene, J. Phys. Chem. B 119 (2015) 8209–8216, https://doi.org/10.1021/acs.jpcb.5b03611.
[61] V.A. Harmandaris, N.P. Adhikari, N.F.A. van der Vegt, K. Kremer, Hierarchical modeling of polystyrene: from atomistic to coarse-grained simulations, Macromolecules 39 (2006) 6708–6719, https://doi.org/10.1021/ma0606399.
[62] V.A. Harmandaris, D. Reith, N.F.A. Van der Vegt, K. Kremer, Comparison between coarse-graining models for polymer systems: Two mapping schemes for polystyrene, Macromol. Chem. Phys. 208 (2007) 2109–2120, https://doi.org/10.1002/macp.200700245.
[63] R. Everaers, S.K. Sukumaran, G.S. Grest, C. Svaneborg, A. Sivasubramanian, K. Kremer, Rheology and microscopic topology of entangled polymeric liquids, Science 303 (2004) 823–826, https://doi.org/10.1126/science.1091215.
[64] Jrg Rottler, Sandra Barsky, Mark, O. Robbins, Cracks and crazes: on calculating the macroscopic fracture energy of glassy polymers from molecular simulations, 148304-148304, Phys. Rev. Lett. 89 (2002), https://doi.org/10.1103/PhysRevLett.89.148304.
[65] Y. Higuchi, K. Saito, T. Sakai, J.P. Gong, M. Kubo, Fracture process of double-network gels by coarse-grained molecular dynamics simulation, Macromolecules 51 (2018) 3075–3087, https://doi.org/10.1021/acs.macromol.8b00124.
[66] M. Formanek, A.J. Moreno, Single-chain nanoparticles under homogeneous shear flow, Macromolecules 52 (2019) 1821–1831, https://doi.org/10.1021/acs.macromol.8b02617.
[67] H.J. Qian, P. Carbone, X.Y. Chen, H.A. Karimi-Varzaneh, C.C. Liew, F. Muller- Plathe, Temperature-transferable coarse-grained potentials for ethylbenzene,

polystyrene, and their mixtures, Macromolecules 41 (2008) 9919–9929, https://doi.org/10.1021/ma801910r.
[68] J.X. Shen, X. Li, L.Q. Zhang, X.S. Lin, H.D. Li, X.J. Shen, V. Ganesan, J. Liu, Mechanical and viscoelastic properties of polymer-grafted nanorod composites from molecular dynamics simulation, Macromolecules 51 (2018) 2641–2652, https://doi.org/10.1021/acs.macromol.8b00183.
[69] J. Shen, X. Lin, J. Liu, X. Li, Effects of cross-link density and distribution on static and dynamic properties of chemically cross-linked polymers, Macromolecules 52 (2019) 121–134, https://doi.org/10.1021/acs.macromol.8b01389.
[70] D. Gersappe, Molecular mechanisms of failure in polymer nanocomposites, Phys. Rev. Lett. 89 (2002), 058301, https://doi.org/10.1103/PhysRevLett.89.058301.
[71] H.X. Wan, K. Gao, S. Li, L.Q. Zhang, X.H. Wu, X.D. Wang, J. Liu, Chemical bond scission and physical slippage in the mullins effect and fatigue behavior of elastomers, Macromolecules 52 (2019) 4209–4221, https://doi.org/10.1021/acs.macromol.9b00128.
[72] S. Bae, O. Galant, C.E. Diesendruck, M.N. Silberstein, Tailoring single chain polymer nanoparticle thermo-mechanical behavior by cross-link density, Soft Matter 13 (2017) 2808–2816, https://doi.org/10.1039/c7sm00360a.
[73] F. Lo Verso, J.A. Pomposo, J. Colmenero, A.J. Moreno, Simulation guided design of globular single-chain nanoparticles by tuning the solvent quality, Soft Matter 11 (2015) 1369–1375, https://doi.org/10.1039/C4SM02475C.
[74] H. Rabbel, P. Breier, J.U. Sommer, Swelling behavior of single-chain polymer nanoparticles: theory and simulation, Macromolecules 50 (2017) 7410–7418, https://doi.org/10.1021/acs.macromol.7b01379.
[75] F. Lo Verso, J.A. Pomposo, J. Colmenero, A.J. Moreno, Tunable slow dynamics in a new class of soft colloids, Soft Matter 12 (2016) 9039–9046, https://doi.org/10.1039/C6SM02136K.
[76] M. Vacatello, Monte Carlo simulations of polymer melts filled with solid nanoparticles, Macromolecules 34 (2001) 1946–1952, https://doi.org/10.1021/ma0015370.
[77] T.H. Zhou, W.H. Ruan, M.Z. Rong, M.Q. Zhang, Y.L. Mai, Keys to toughening of non-layered nanoparticles/polymer composites, Adv. Mater. 19 (2007) 2667–2671, https://doi.org/10.1002/adma.200602611.
[78] J. Wang, X. Jin, C. Li, W. Wang, H. Wu, S. Guo, Graphene and graphene derivatives toughening polymers: Toward high toughness and strength, Chem. Eng. J. 370 (2019) 831–854, https://doi.org/10.1016/j.cej.2019.03.229.